PAPER

NJC
www.rsc.org/njc

Synthesis and characterization of magnetic organic-inorganic nanocomposites based on the $[Mn_2O_{12}\{CH_2C(CH_3)COO\}_{16}(H_2O)_4]$ building block†

Stephanie Willemin,[a] Bruno Donnadieu,[b] Lollita Lecren,[c] Bernard Henner,[a] Rodolphe Clérac,[c] Christian Guérin,[a] Albert Meyer,[d] Alexander V. Pokrovskii[e] and Joulia Larionova*[a]

[a] *Laboratoire de Chimie Moléculaire et Organisation du Solide (LCMOS; CNRS UMR 5637), Université Montpellier II, Place E. Bataillon, CC 007, 34095, Montpellier cedex 5, France. E-mail: joulia@univ-montp2.fr; Fax: +33 4 67 14 38 52*
[b] *Laboratoire de Chimie de Coordination (LCC; CNRS UPR 8241), CNRS, 205 Route de Narbonne, 31077, Toulouse cedex 4, France*
[c] *Centre de Recherche Paul Pascal (CRPP; CNRS UPR 864, CNRS, 115 avenue du Dr. A. Schweitzer, 33600, Pessac, France*
[d] *Laboratoire de Chimie Organique Biomoléculaire de Synthèse (CNRS UMR 5625), Université Montpellier II, Place E. Bataillon, CC 008, 34095, Montpellier cedex 5, France*
[e] *Technology University of St. Petersburg, Moskovskii 26, 195274, St. Petersburg, Russia*

Received* (*in Montpellier, France*) *10th February 2004, Accepted 7th April 2004
First published as an Advance Article on the web 21st July 2004

The new methacrylate-substituted manganese carboxylate cluster $[Mn_{12}O_{12}\{CH_2C(CH_3)COO\}_{16}(H_2O)_4]$ having single molecule magnetic (SMM) properties was synthesized and fully characterized by X-ray crystallography, LDI-TOF, fast atom bombardment (FAB) analyses and magnetic measurements. This cluster, containing sixteen polymerizable functionalities, was used as a cross-linker in the radical copolymerization with methyl methacrylate monomer in order to obtain hybrid cross-linked copolymers. The obtained nanocomposites were studied by infrared spectroscopy, magnetic measurements, thermogravimetric analysis, differential scanning calorimetry and transmission electronic microscopy. All these methods, along with the study of the swelling properties, reveal that the intact manganese cluster is enwrapped and covalently bonded to the polymer matrix, allowing to improve its chemical and thermal stability. The resulting nanocomposite materials have SMM properties.

Introduction

Polymeric organic-inorganic nanocomposites include a special class of hybrid materials originating from intimate combinations of inorganic nanoparticles or nanoclusters with polymers, resulting in materials that exhibit unique physical properties.[1] These nanocomposites have attracted a great deal of attention in the field of materials science because their properties can be derived from the successful combination of the characteristics of the parent constituents into a single material. The use of polymers as matrixes adds flexibility to the system and endows nanocomposite materials with good processability, which is important for technological applications. In addition, the polymeric matrixes can provide specific mechanical, rheological, optical, conducting or electrical properties, which can be taken together with the unique properties of the nanosized objects. Indeed, polymeric nanocomposites have found successful applications in various areas, including optics,[2] microelectronics,[3] biology,[4] sensors[5] and catalysis.[6]

Many investigations regarding the development of the incorporation techniques of nanoparticles into polymeric matrixes have been published.[1–7] In most of the cases, such combinations require blending or mixing of inorganic species, such as metal or metal oxide nanoparticles with organic polymers, using the latter in solution or in a melt form.[7] Recently discovered soft chemistry processes offer interesting approaches to the chemical design of hybrid nanocomposites in which inorganic components at the nanosize level and polymeric matrixes are covalently linked.[8] One of these approaches consists in the copolymerization of well-defined inorganic nanoclusters containing polymerizable functionalities with organic polymers in hybrid copolymer networks.[9] Several acrylate- and methacrylate-substituted clusters, such as siloxane,[10] stannoxane,[11] oxo-zirconate,[12] oxo-titanate,[13] oxo-molybdate[14] and oxo-tungstate[15] offering interesting optical and catalytic properties, have been used as cross-linkers in the copolymerization with methyl methacrylates in order to design hybrid copolymers. In these systems, functionalized clusters act as nanobuilding blocks and cross-linkers in order to create covalently cross-linked networks. The nanostructure, degree of organization and properties of these copolymers depend on the chemical nature of their components and may also depend on the synergy between these components.

Manganese oxide clusters of general formula $[Mn_{12}O_{12}(RCOO)_{16}(H_2O)_4]$ (R = alkyl, aryl) present remarkable magnetic properties, which are called single-molecule magnetic

† Electronic supplementary information (ESI) available: figures showing the IR spectrum, molecular packing, FAB-MS spectrum and field dependence of the magnetization of $[Mn_{12}O_{12}\{CH_2C(CH_3)COO\}_{16}(H_2O)_4]\cdot 4CH_2C(CH_3)COOH\cdot CH_2Cl_2$, as well as the IR spectrum of the $R = 200$ copolymer and a plot of T_g as a function of R for the copolymers. See http://www.rsc.org/suppdata/nj/b4/b402080d/

DOI: 10.1039/b402080d

(SMM) behaviour.[16] These molecules have a large spin ground state together with a strong uniaxial anisotropy, resulting in an energy barrier for spin reversal.[17] This feature is characterized by a slow relaxation of the magnetization, which gives rise to a "metastable magnet" with out-of-phase ac magnetic susceptibility signals and stepwise hysteresis effects similar to those observed in bulk magnets.[18] Additionally, these molecules display quantum tunnelling of the magnetization and quantum phase interference. Therefore, these clusters can be represented as superparamagnetic particles of a sharply defined size that may offer new possibilities for high-density information storage, at the molecular level, and quantum-computing applications.

In recent years, an important effort has been focused on the design of nanocomposite materials based on magnetic clusters in order to control the dispersion of these individual molecules or molecular aggregates into organic or inorganic matrixes. Indeed, the dispersion of $[Mn_{12}O_{12}(RCOO)_{16}(H_2O)_4]$ molecules into organized multilayered Langmuir–Blodgett films[19] and polymeric thin film[20] has recently been reported. Hexagonal mesoporous silica hosts have also been used for the incorporation of manganese carboxylate clusters on the nanometer scale into the one-dimensional channels.[21] In all of these reported approaches, the cluster molecules are randomly dispersed inside organic or inorganic matrixes and host-guest interactions may be considered as very small or negligible. To the best of our knowledge, SMM clusters have never been used as building blocks and cross-linkers in designing hybrid copolymer networks. This approach should allow the preparation of magnetic organic-inorganic hybrid copolymers in which a polymer matrix will enwrap and protect cluster molecules in order to improve their chemical and/or thermal stability. The covalent bond between the cluster and the organic matrix may allow the control and modulation of the polymer-to-cluster ratio. Moreover, the possibility of varying the number of polymerizable functionalities of the magnetic cluster and the polymer-to-cluster ratio should allow us to modify the morphology and physical properties of hybrid copolymers. In addition, this approach should favour the processability of these materials. Here we report the synthesis, the characterization and the study of the physical properties of polymer-based nanocomposites containing a methacrylate-substituted high-spin manganese carboxylate cluster $[Mn_{12}O_{12}\{CH_2C(CH_3)COO\}_{16}(H_2O)_4]$ covalently bonded to the polymeric matrix.

Experimental

All chemicals and solvents were used as received. Methyl methacrylate (MMA) was treated with a 4% solution of K_2CO_3 in order to remove the stabilizer. All preparations and manipulations were done under aerobic conditions. $[Mn_{12}O_{12}(CH_3COO)_{16}(H_2O)_4]\cdot 4H_2O\cdot 2CH_3COOH$ was prepared as previously described.[22]

Syntheses

Cluster $[Mn_{12}O_{12}\{CH_2C(CH_3)COO\}_{16}(H_2O)_4]\cdot 4CH_2C(CH_3)COOH\cdot CH_2Cl_2$. To a slurry of complex $[Mn_{12}O_{12}(CH_3COO)_{16}(H_2O)_4]\cdot 4H_2O\cdot 2CH_3COOH$ (1.0 g; 0.49 mmol) in 50 mL of toluene was added $HO_2C(CH_3)CCH_2$ (0.137 g, 16 mmol). The solution was allowed to stir for 1 h. Then, the mixture was concentrated under vacuum to remove the acetic acid. The resulting solid and additional $HO_2C(CH_3)CCH_2$(0.137 g, 16 mmol) were dissolved in toluene (50 mL), stirred 1 h and then concentrated to remove the acetic acid. In order to substitute all of the acetate ligands, this procedure was repeated once more. The resulting brown powder was recrystallized by slow diffusion of hexane into a CH_2Cl_2 solution of the complex. Brown crystals suitable for structural determination by X-ray crystallography were obtained after 24 h. Yield: 65%. Elem. anal. calcd for $C_{81}H_{114}Cl_2Mn_{12}O_{56}$: C, 35.82; H, 4.20; Cl, 2.61; Mn, 24.32%; found: C, 36.53; Cl, 2.57; H, 4.33; Mn, 24.36. IR (cm^{-1}, KBr disk): ν(C=C) 1635(w), ν_{as}(OCO) 1560(m), ν_{as}(OCO) 1419(s), δ(C–H) 941(m), ν(Mn–O) 626(m).

Poly(methyl methacrylate) (PMMA). 2,2′-Azobis(isobutyronitrile) (AIBN; 0.032 g, 2×10^{-4} mol) and two drops of dibutylphthalate (DBPh; 0.048 g, 1.72×10^{-4} mol) were added to MMA (1 g, 1×10^{-2} mol). The reaction mixture was heated to 60 °C under vacuum in a sealed tube for 48 h. The obtained PMMA is a transparent glassy solid. IR (cm^{-1}): ν(C=O) 1721(vs), ν(C–O) 1140(vs).

Hybrid copolymers. The copolymers were obtained by radical-initiated copolymerization of the cluster with MMA. A typical synthesis was performed as follows: $[Mn_{12}O_{12}\{CH_2C(CH_3)COO\}_{16}(H_2O)_4]\cdot 4CH_2C(CH_3)COOH\cdot CH_2Cl_2$ was dissolved in a mixture of DBPh (two drops) and MMA (1 g, 1×10^{-2} mol) at room temperature and then the brown solution was filtered. AIBN (0.035 g, 2.32×10^{-4} mol) was added and the reaction mixture was heated to 60 °C under vacuum in a sealed tube for 48 h. The brown solids were washed several times with THF and then dried *in vacuo*. Six copolymers with different molar ratios, $R = n(\text{MMA})/n(\text{cluster})$, equal to 100, 200, 300, 500, 800 and 1000 were synthesized. The quantities of the cluster used for the syntheses were: for $R = 100$, 0.265 g (1×10^{-4} mol); $R = 200$, 0.132 g (5×10^{-5} mol); $R = 300$, 0.088 g (3.33×10^{-5} mol); $R = 500$, 0.053 g (2×10^{-5} mol); $R = 800$, 0.033 g (1.25×10^{-5} mol); $R = 1000$, 0.026 g (1×10^{-5} mol). Percadox-16S was also employed as initiator instead of AIBN. In this case, the same procedure was used, but the reaction mixture was heated to 40 °C.

Copolymer R = 100. Elem. anal. calcd for $C_{64}H_{80}Mn_{12}O_{44}/100(C_5H_8O_2)$: C, 55.42; H, 7.20; Mn, 5.40%; found: C, 55.61; H, 7.10; Mn, 5.22. IR (cm^{-1}, KBr disk): ν(C = O) 1732(vs), ν(C=C) 1638(vw), ν_{as}(OCO) 1562(m), ν_s(OCO) 1421(m), ν(C–O) 1150(vs), ν(Mn–O) 633(m).

Copolymer R = 200. Elem. anal. calcd for $C_{64}H_{80}Mn_{12}O_{44}/200(C_5H_8O_2)$: C, 57.48; H, 7.56; Mn, 2.97%; found: C, 57.69; H, 7.77; Mn, 2.43. IR (cm^{-1}, KBr disk): ν(C=O) 1731(vs), ν(C–C) 1638(vw), ν_{as}(OCO) 1563(m), ν_s(OCO) 1430(m), ν(C–O) 1149(vs), ν(Mn–O) 635(m).

Copolymer R = 300. Elem. anal. calcd for $C_{64}H_{80}Mn_{12}O_{44}/300(C_5H_8O_2)$: C, 58.26; H, 7.69; Mn, 2.04%; found: C, 58.41; H, 7.40; Mn, 2.21. IR (cm^{-1}, KBr disk): ν(C=O) 1729(vs), ν(C=C) 1638(vw), ν_{as}(OCO) 1560(m), ν_s(OCO) 1451(m), ν(C–O) 1148(s), ν(Mn–O) 629(vw).

Copolymer R = 500. Elem. anal. calcd for $C_{64}H_{80}Mn_{12}O_{44}/500(C_5H_8O_2)$: C, 58.92; H, 7.81; Mn, 1.26%; found: C, 58.69; H, 7.90; Mn, 1.02. IR (cm^{-1}, KBr disk): ν(C=O) 1729(vs), ν(C=C) 1638(vw), ν_{as}(OCO) 1563(m), ν_s(OCO) 1451(s), ν(C–O) 1149(s), ν(Mn–O) 629(vw).

Copolymer R = 800. Elem. anal. calcd for $C_{64}H_{80}Mn_{12}O_{44}/800(C_5H_8O_2)$: C, 59.31; H, 7.89; Mn, 0.80%; found: C, 59.55; H, 8.17; Mn, 0.61. IR (cm^{-1}, KBr disk): ν(C=O) 1731(vs), ν(C=C) 1638(vw), ν_{as}(OCO) 1560(m), ν_s(OCO) 1450(s), ν(C–O) 1148(vs), ν(Mn–O) 629(vw).

Copolymer R = 1000. Elem. anal. calcd for $C_{64}H_{80}Mn_{12}O_{44}/1000(C_5H_8O_2)$: C, 59.79; H, 7.96; Mn, 0.65%; found: C, 59.96; H, 8.07; Mn, 0.61. IR (cm^{-1}, KBr disk):ν(C=O) 1728(vs), ν(C=C) 1638(vw), ν_{as}(OCO) 1560(m), ν_s(OCO) 1451(s), ν(C–O) 1145(vs), ν(Mn–O) 600(vw).

X-Ray crystallographic studies of $[Mn_{12}O_{12}\{CH_2C(CH_3)COO\}_{16}(H_2O)_4]\cdot 4CH_2C(CH_3)COOH\cdot CH_2Cl_2$

Data were collected at low temperature ($T = 100$ K) on a four-circle Kappa CCD Xcalibur Oxford diffractometer, using graphite-monochromated Mo-Kα radiation ($\lambda = 0.71073$ Å) and equipped with an Oxford Instruments Cryogenic Nitrogen jet Cooler Device. Numerical absorption corrections were applied using the CrysAlis System (RED Version 1.170.14; release 21.11.2002 CrysAlis170). The final unit cell parameters have been obtained by means of a least-squares refinement performed on a set of 8000 well-measured reflections and the crystal decay has been monitored. No significant fluctuations of intensities were observed during the data collection. The crystallographic data for $[Mn_{12}O_{12}\{CH_2C(CH_3)COO\}_{16}(H_2O)_4]\cdot 4CH_2C(CH_3)COOH\cdot CH_2Cl_2$ are listed in Table 1. The structure has been solved by direct methods using SIR92[23] followed by Fourier synthesis and refined by means of least-squares procedures on F^2 (SHELXL97).[24] The atomic scattering factors were taken from the International Tables for X-Ray Crystallography.[25] The hydrogen atoms of the methacrylate ligands and molecules of methacrylic acid were located on difference Fourier maps and idealized positions were introduced in the refinement. The C–H distances were fixed at 0.93 and 0.96 Å for C(sp^2) and C(sp^3) atoms, respectively. The isotropic parameters were fixed higher than the U_{eq} values by 20% and 50% for C(sp^2) and C(sp^3) atoms, respectively. Methyl groups were refined by using a specific model, with the torsion angle as a free variable. The hydrogen atoms H(102) and H(201) connected to –COOH groups of the two methacrylic acid molecules were isotropically refined. For the hydrogen atoms H(11w), H(12w) and H(21w), H(22w) connected to oxygen atoms O(1w) and O(2w), respectively, their coordinates were calculated using the modelling program HYDROGEN.[26] This program uses a combination of geometric inspections of the environments of H_2O molecules and force field calculations on the basis of hydrogen-bonding interactions. Consequently, coordinates of these hydrogen atoms were not refined and $U_{[iso]}$ were fixed at 20% higher than those of the oxygen atoms to which they were connected. A molecule of dichloromethane was located and found to be strongly disordered. Some restraints put on the interatomic distances and angles were used in order to get a chemically reasonable model. All non-hydrogen atoms were anisotropically refined and in the last cycles of refinement a weighting scheme has been used. Criteria for a satisfactory complete analysis were the ratios of root mean square shift standard deviations being less than 0.1 with no significant features in final difference Fourier maps.‡

Table 1 Crystal data and structure refinement for $[Mn_{12}O_{12}\{CH_2C(CH_3)COO\}_{16}(H_2O)_4]\cdot 4CH_2C(CH_3)COOH\cdot CH_2Cl_2$.

Empirical formula	$C_{81}H_{114}Cl_2O_{56}Mn_{12}$
Formula weight	2711.9
Temperature/K	100(2)
Wavelength/Å	0.71073
Crystal system	Monoclinic
Space group	$C2/c$ (no. 15)
a/Å	30.445(6)
b/Å	14.098(3)
c/Å	29.300(6)
β/°	116.28(3)
U/Å^3	11 276(4)
Z	4
Absorption coefficient/mm^{-1}	1.422
Reflections collected	83 421
Unique reflections	11 358
R_{int}	0.0414
R_1 [$I > 2\sigma(I)$]	0.0402
wR_2 [$I > 2\sigma(I)$][a]	0.0904
R_1 (all data)	0.0456
wR_2 (all data)[a]	0.0931

[a] Weighing scheme: $w = 1/[\sigma^2(F_o^2) + (0.0295P)^2 + 63.207P]$ where $P = (F_o^2 + 2F_c^2)/3)$

Physical measurements

Infrared spectra were recorded in KBr disks on a Nicolet model 510 P spectrophotometer and on a Perkin Elmer 2000 spectrophotometer equipped with attenuated total reflectance (FTIR-ATR Benchmark "In compartment" with ZnSe platine) with 4 cm^{-1} resolution. Thermogravimetry analyses (TGA) were performed using a Netzsch STA 409 instrument under air or argon from 25 to 700 °C at a heating rate of 2 °C min^{-1}. Differential scanning calorimetry (DSC) was performed using a Mettler Toledo Star SSW 7.01 instrument under nitrogen from 25 to 150 °C at a heating rate of 10 °C min^{-1}. Spontaneous cooling has been performed under nitrogen atmosphere. It was used to evaluate any enthalpic events and to monitor glass transition temperatures (T_g). Laser desorption/ionization time-of-flight mass spectra (LDI-TOF MS) were recorded with an Applied Biosystems Voyager System 1104 mass spectrometer equipped with a nitrogen laser (337 nm) without matrices. LDI conditions: accelerating voltage, 24 000 V; guide wire, 0.05% of accelerating voltage; grid voltage, 94% of accelerating voltage; delay extraction time is of 550 ns. The samples were prepared by dissolving the cluster in an approximately 1:100 ratio in CH_3CN and then applying a 2 µL sample of the solution onto the stainless steel sample holders used in the instrument. The samples were run immediately after air-drying at room temperature. Fast atom bombardment (FAB) analyses were recorded with a JEOL DX300 mass spectrometer. Nitrobenzyl alcohol was used as a matrix for the measurements. Magnetic susceptibility data were collected with a Quantum Design MPMS-XL SQUID magnetometer in a temperature range of 1.8–350 K and up to 7 T. Ac measurements were performed in 0.3 mT ac field with an ac frequency ranging from 1 to 1500 Hz without dc field. Experimental data were corrected for the sample holder and for diamagnetic contributions calculated from Pascal constants.[27] Transmission electron microscopy (TEM) has been performed on a JEOL 1200 EXII working at 100 kV. Samples for TEM measurements were prepared using ultramicrotomy techniques. Elemental analyses were performed by the Service Central d'Analyses (CNRS, Vernaison, France).

Characterization of the degree of swelling

The samples of copolymers were placed in an appropriate solvent and allowed to equilibrate for 1 day at 25 °C. Equilibrium was attained when the weight of the swollen copolymer remained constant. The samples were then dried *in vacuo* at 40 °C in order to obtain the weight of the dried copolymer. The swelling index, I_{sw}, can be calculated at the swelling equilibrium at 25 °C according to the formula: $I_{sw} = 100\cdot(M_{wet} - M_{dry})/M_{dry}$, where M_{wet} is the weight of the swollen copolymer gel and M_{dry} is the weight of the dry copolymer.[28] All degrees of swelling were determined in triplicate and the average values are presented.

‡ CCDC reference number 210936. See http://www.rsc.org/suppdata/nj/b4/b402080d/ for crystallographic data in .cif or other electronic format.

Results and discussion

Synthesis and characterization of the methacrylate-substituted $[Mn_{12}O_{12}\{CH_2C(CH_3)COO\}_{16}(H_2O)_4]\cdot 4CH_2C(CH_3)COOH\cdot CH_2Cl_2$ cluster

$[Mn_{12}O_{12}[CH_2C(CH_3)COO\}_{16}(H_2O)_4]\cdot 4CH_2C(CH_3)COOH\cdot CH_2Cl_2$ was prepared in 65% yield *via* a ligand exchange reaction as summarized in eqn. (1):

$$[Mn_{12}O_{12}(CH_3COO)_{16}(H_2O)_4] + 16CH_2C(CH_3)COOH \leftrightarrows [Mn_{12}O_{12}\{CH_2C(CH_3)COO\}_{16}(H_2O)_4] + 16CH_3COOH \quad (1)$$

As usually observed in the case of such reactions, the two clusters in equilibrium are both likely present in solution.[29] The complete substitution of $[Mn_{12}O_{12}(CH_3COO)_{16}(H_2O)_4]\cdot 2CH_3COOH\cdot 4H_2O$ was achieved by two successive treatments with a 2 molar-fold excess of the methacrylic acid and the acetic acid was removed from the reaction mixture by vacuum distillation.

The infrared spectrum of $[Mn_{12}O_{12}\{CH_2C(CH_3)COO\}_{16}(H_2O)_4]\cdot 4CH_2C(CH_3)COOH\cdot CH_2Cl_2$ (Fig. 1S, ESI) exhibits the low frequency bands of the cluster in the 500–800 cm^{-1} range (455, 551, 626, 665 and 714 cm^{-1}) corresponding to Mn–O stretches of the cluster core. The regions around 1560 and 1420–1450 cm^{-1} exhibit the antisymmetrical and symmetrical OCO stretches, respectively, of carboxylate ligands in their usual syn, syn bidentate bridging mode.[30] The IR spectrum shows also the ν(C=C) absorption at 1635 and δ(C–H) absorption of $-C(CH_3)CH_2$ at 940 cm^{-1}, characteristic of the double bonds of the coordinated methacrylate ligands.

Single crystal X-ray structure analysis performed at 100 K revealed that this compound crystallizes in the monoclinic space group $C2/c$ (no. 15) (Table 1). Four molecules of methacrylic acid and one molecule of CH_2Cl_2 are present in the unit cell. Fig. 1 shows the molecular structure of $[Mn_{12}O_{12}\{CH_2C(CH_3)COO\}_{16}(H_2O)_4]\cdot 4CH_2C(CH_3)COOH\cdot CH_2Cl_2$ along the crystallographic *a* axis. The $Mn_{12}O_{12}$ core structure is similar in many respects to the previously described $[Mn_{12}O_{12}(RCOO)_{16}(H_2O)_4]$ compounds.[29] The central $[Mn^{IV}_4O_4]$ cube-like core is surrounded by a non-planar ring of eight outer Mn^{III} ions that are bridged and connected to the cube *via* μ_3-O^{2-} ions. The peripheral ligation is achieved by sixteen bridging methacrylate ligands, eight in equatorial and eight in axial positions, and four terminal water molecules. The arrangement of the latter is in a 1:1:1:1 fashion with alternating up and down positions.

Table 2 lists the average Mn–O bond lengths around each manganese ion. The average value of the six Mn–O bond lengths for the Mn^{4+} ions is quite short and equal to 1.86 Å. On the other hand, the Mn–O bonds of the Mn^{3+} ions are divided into two groups, equatorial bonds (1.89–1.98 Å) and axial ones (2.11–2.22 Å), which are about 10% longer. This elongation of axial Mn–O bond lengths compared to the equatorial ones is caused by the Jahn–Teller distortion in Mn^{3+} ions. The four water oxygen atoms are involved in the lengthening of the Mn–O bonds. The eight Jahn–Teller axes form angles of 15–40° with the crystallographic *b* axis.

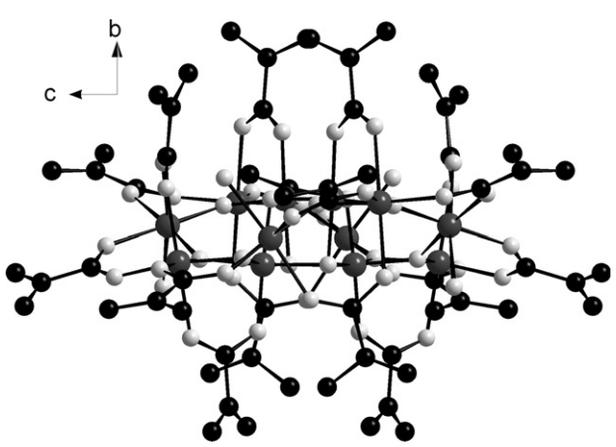

Fig. 1 Crystal structure of the $[Mn_{12}O_{12}\{CH_2C(CH_3)COO\}_{16}(H_2O)_4]$ unit along the crystallographic *a* axis. Hydrogen atoms and solvent molecules have been omitted for clarity.

Table 2 Selected bond distances (Å) for $[Mn_{12}O_{12}\{CH_2C(CH_3)COO\}_{16}(H_2O)_4]\cdot 4CH_2C(CH_3)COOH\cdot CH_2Cl_2$.

Mn(1)–O(17)	1.8202(19)	Mn(1)–O(18)	1.8975(19)
Mn(1)–O(6)	1.952(2)	Mn(1)–O(1)	1.976(2)
Mn(1)–O(3)	2.114(2)	Mn(1)–O(1W)	2.188(2)
Mn(2)–O(18)	1.8594(19)	Mn(2)–O(19)	1.9057(19)
Mn(2)–O(13)	1.940(2)	Mn(2)–O(5)	1.948(2)
Mn(2)–O(16)	2.162(2)	Mn(2)–O(12)	2.220(2)
Mn(3)–O(19)	1.8792(19)	Mn(3)–O(18)	1.8594(19)
Mn(3)–O(20)	1.9305(19)	Mn(3)–O(21)	1.8980(18)
Mn(3)–O(11)	1.9475(19)	Mn(3)–O(20)#1	1.9305(19)
Mn(4)–O(22)	1.8638(19)	Mn(4)–O(17)	1.8854(19)
Mn(4)–O(20)	1.9076(18)	Mn(4)–O(21)#1	1.9354(18)
Mn(4)–O(21)	1.9387(18)	Mn(4)–O(10)	1.9414(19)
Mn(5)–O(17)	1.9066(19)	Mn(5)–O(22)	1.8935(19)
Mn(5)–O(7)	1.945(2)	Mn(5)–O(2)	1.943(2)
Mn(5)–O(9)	2.229(2)	Mn(5)–O(4)	2.178(2)
Mn(6)–O(22)#1	1.904(2)	Mn(6)–O(19)	1.8859(19)
Mn(6)–O(14)	1.984(2)	Mn(6)–O(8)#1	1.956(2)
Mn(6)–O(2W)	2.182(2)	Mn(6)–O(15)	2.122(2)

The cluster in the molecular packing of the unit cell (Fig. 2S, ESI) appears to possess a number of weak intermolecular hydrogen bonds, involving C–H···O, O–H···O and C–H···Cl interactions of the cluster molecules with $CH_2C(CH_3)COOH$ and of the cluster molecules with CH_2Cl_2 interstitial solvent molecules. There are O–H···O and C–H···O interactions with O···O and C···O distances of 2.766–3.979 Å (with a mean value of 3.328 Å) and 3.379–3.921 Å (with a mean value of 3.478 Å), respectively, and C–H···Cl interactions with C···Cl distances of 3.795 Å. These values are typical of these types of hydrogen-bonding contacts.[31]

The LDI-TOF mass spectrometric technique provides an accurate determination of the molecular mass of carboxylate clusters.[32] The mass spectrum of $[Mn_{12}O_{12}\{CH_2C(CH_3)COO\}_{16}(H_2O)_4]\cdot 4CH_2C(CH_3)COOH\cdot CH_2Cl_2$ has been recorded without matrix because the cluster has an absorption at the wavelength of the laser source (337 nm). The high mass region (above 500 Da) of the LDI-TOF mass spectrum recorded in positive mode (Fig. 2, top) reveals only one series of well-distinguished peaks. The first one at $m/z = 2211$ corresponds to the molecular ion $[Mn_{12}O_{12}\{CH_2C(CH_3)COO\}_{16}]^+$. Obviously, the molecules of crystallization $[CH_2C(CH_3)COOH$ and $CH_2Cl_2]$ and the four coordinated water molecules initially present in the cluster have been removed under the high vacuum conditions used for the experiments. The observed sequence of peaks (2126, 2041, 1956, 1871 and 1786 m/z) corresponds to the stepwise loss of one methyl methacrylate unit ($\Delta m = 85$): $[Mn_{12}O_{12}\{CH_2C(CH_3)COO\}_{15}]^+$ ($m/z = 2126$), $[Mn_{12}O_{12}\{CH_2C(CH_3)COO\}_{14}]^+$ ($m/z = 2041$), $[Mn_{12}O_{12}\{CH_2C(CH_3)COO\}_{13}]^+$ ($m/z = 1956$), $[Mn_{12}O_{12}\{CH_2C(CH_3)COO\}_{12}]^+$ ($m/z = 1871$), $[Mn_{12}O_{12}\{CH_2C(CH_3)COO\}_{11}]^+$ ($m/z = 1786$). Furthermore, the high-mass region of the LDI-TOF mass spectrum recorded in negative mode (Fig. 2, bottom) also shows only one series of peaks (2210, 2124, 2040, 1954, 1870, 1784 m/z), which can be assigned to the sequence $[Mn_{12}O_{12}\{CH_2C(CH_3)COO\}_{16}]^-$ ($m/z = 2211$), $[Mn_{12}O_{12}\{CH_2C(CH_3)COO\}_{15}]^-$ ($m/z = 2126$), $[Mn_{12}O_{12}\{CH_2C(CH_3)COO\}_{14}]^-$ ($m/z = 2041$),

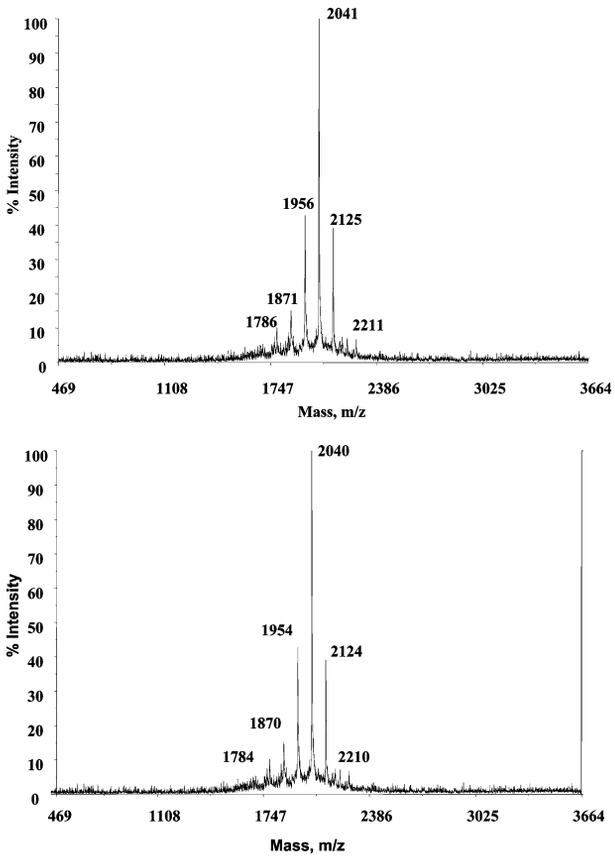

Fig. 2 High mass region of the LDI-TOF mass spectra of $[Mn_{12}O_{12}\{CH_2C(CH_3)COO\}_{16}(H_2O)_4]\cdot 4CH_2C(CH_3)COOH\cdot CH_2Cl_2$ recorded in positive (top) and negative (bottom) modes.

$[Mn_{12}O_{12}\{CH_2C(CH_3)COO\}_{13}]^-$ ($m/z = 1956$), $[Mn_{12}O_{12}\{CH_2C(CH_3)COO\}_{12}]^-$ ($m/z = 1871$), $[Mn_{12}O_{12}\{CH_2C(CH_3)COO\}_{11}]^-$ ($m/z = 1786$). The same distribution of peak intensities with the most significant peaks attributed to the fragments $[Mn_{12}O_{12}\{CH_2C(CH_3)COO\}_{14}]^+$ and $[Mn_{12}O_{12}\{CH_2C(CH_3)COO\}_{14}]^-$ is present in the positive and the negative modes, respectively, and is common to all of the clusters already studied by the MALDI-TOF technique.[31] Clearly, starting from $[Mn_{12}O_{12}\{CH_2C(CH_3)COO\}_{16}]^+$, the sequent loss of methyl methacrylate units leads to the formation of fragments $[Mn_{12}O_{12}\{CH_2C(CH_3)COO\}_{16-n}]^+$, which are observed in the positive ion mode spectra. As proposed previously,[32] the formation of the series of negative fragments $[Mn_{12}O_{12}\{CH_2C(CH_3)COO\}_{16-n}]^-$ detected in the negative ion mode spectra may probably originate from a disproportionation of neutral fragments $[Mn_{12}O_{12}\{CH_2C(CH_3)COO\}_{16-n}]$, leading to $[Mn_{12}O_{12}\{CH_2C(CH_3)COO\}_{16-n}]^+$ and $[Mn_{12}O_{12}\{CH_2C(CH_3)COO\}_{16-n}]^-$. An oxidative decarboxylation of the latter may lead to $[Mn_{12}O_{12}\{CH_2C(CH_3)COO\}_{15-n}]^-$ while the loss of a carboxylate anion may lead to the neutral $[Mn_{12}O_{12}\{CH_2C(CH_3)COO\}_{15-n}]$.

The FAB analysis, using NBA as the matrix, performed in negative and positive modes on $[Mn_{12}O_{12}\{CH_2C(CH_3)COO\}_{16}(H_2O)_4]\cdot 4CH_2C(CH_3)COOH\cdot CH_2Cl_2$ (Fig. 3S, ESI) confirms the structure. In both modes, the first observed peaks are at 2285 and 2283 m/z, which correspond to the molecular entities $[Mn_{12}O_{12}\{CH_2C(CH_3)COO\}_{16}(H_2O)_4]^+$ or $[Mn_{12}O_{12}\{CH_2C(CH_3)COO\}_{16}(H_2O)_4]^-$, respectively. As expected, the molecules of crystallization of methacrylic acid and CH_2Cl_2 are not conserved after solubilization of the cluster in NBA and as a consequence cannot be viewed in the FAB spectra. However, in contrast to the LDI-TOF analysis, the FAB experiment does not require high vacuum conditions. As a consequence, the presence of the four coordinated water molecules in the molecular entity has been detected. The spectrum in the positive mode shows a sequence of nine peaks at 2282, 2210, 2126, 2041, 1956, 1877, 1786, 1701, 1616 m/z, which can be attributed to the entities $[Mn_{12}O_{12}\{CH_2C(CH_3)COO\}_{16}(H_2O)_4]^+$, the fragments $[Mn_{12}O_{12}\{CH_2C(CH_3)COO\}_{16-n}]^+$ (with n varying from 0 to 7) obtained by the stepwise loss of the methyl methacrylate unit $CH_2C(CH_3)COO^\bullet$ ($\Delta m/z = 85$). A similar situation is observed in the negative mode spectrum. The observed peaks (2282, 2209, 2125, 2040, 1955, 1876, 1785, 1700 and 1615 m/z) can also be attributed to the entities $[Mn_{12}O_{12}\{CH_2C(CH_3)COO\}_{16}(H_2O)_4]^-$ and the fragments $[Mn_{12}O_{12}\{CH_2C(CH_3)COO\}_{16-n}]^-$ (n varies from 0 to 7). As observed in the case of LDI-TOF experiment, the most intense peaks in the FAB experiments correspond to the fragments $[Mn_{12}O_{12}\{CH_2C(CH_3)COO\}_{14}]^z$ ($z = +1$ or -1).

The thermogravimetric analysis of $[Mn_{12}O_{12}\{CH_2C(CH_3)COO\}_{16}(H_2O)_4]\cdot 4CH_2C(CH_3)COOH\cdot CH_2Cl_2$ was performed under argon from room temperature up to 700 °C with a heating rate of 2 °C min^{-1}, as shown in Fig. 3. The thermogravimetric curve exhibits four weight losses with inflection points at 73, 111, 160 and 380 °C, as the temperature was increased. The three first weight loss steps of 3.3, 6.5 and 3.3% correspond to the successive losses of one, two and one molecules of crystallized methacrylic acid. Visibly, the CH_2Cl_2 of crystallization initially present in the cluster has been removed in the early stage of the experiment by the flow of argon. The loss of all crystallization molecules leads to the cluster $[Mn_{12}O_{12}\{CH_2C(CH_3)COO\}_{16}(H_2O)_4]$.[33] The thermogravimetric analyses performed under air shows that the cluster starts to decompose at 160 °C and the formation of Mn_3O_4, proved by X-ray powder diffraction analysis and magnetic measurements, is observed at 600 °C.[34]

The magnetic properties of $[Mn_{12}O_{12}\{CH_2C(CH_3)COO\}_{16}(H_2O)_4]\cdot 4CH_2C(CH_3)COOH\cdot CH_2Cl_2$ were studied in ac and dc modes on polycrystalline samples. The temperature dependence of the in-phase, χ', and out-of-phase, χ'', components of the ac susceptibility were measured in a zero external field with different frequencies ranging from 1 to 1500 Hz (Fig. 4). At 1 Hz, both χ' and χ'' responses exhibit a single peak at 4.5 and 4.0 K, respectively, which shift towards higher temperature when the frequency increases. This feature is characteristic of superparamagnetic-like behaviour (or SMM behaviour).[16,17] The frequency dependence of these peaks can be analysed by the Arrhenius law, $\tau = \tau_0 \exp(\Delta/k_BT)$, as shown in Fig. 5.

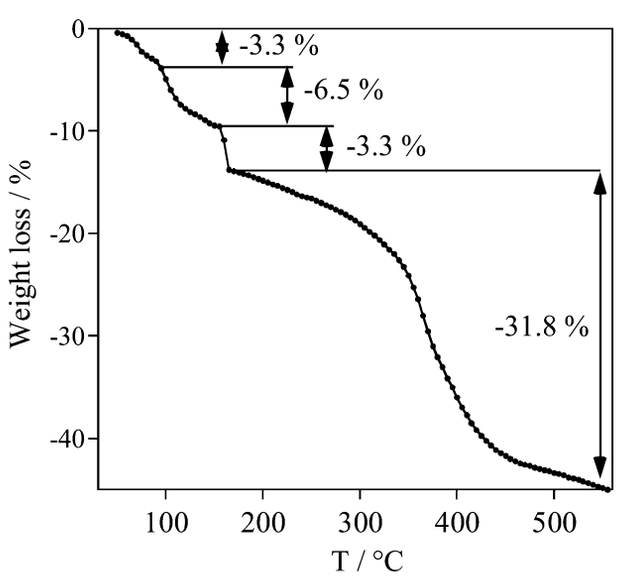

Fig. 3 Thermogravimetric analysis of $[Mn_{12}O_{12}\{CH_2C(CH_3)COO\}_{16}(H_2O)_4]\cdot 4CH_2C(CH_3)COOH\cdot CH_2Cl_2$.

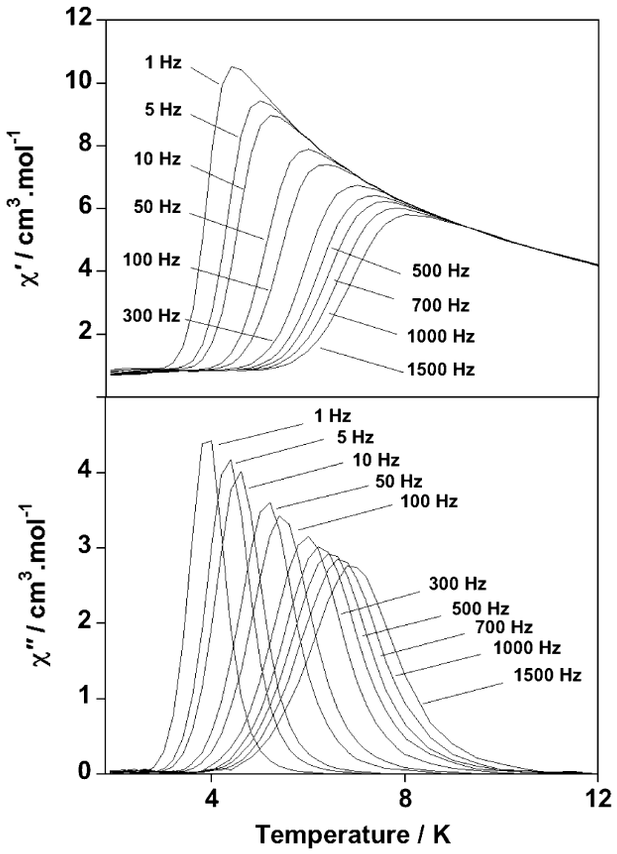

Fig. 4 Temperature and frequency dependence of the (top) real (χ'_M) and (bottom) imaginary (χ''_M) parts of the ac susceptibility for $[Mn_{12}O_{12}\{CH_2C(CH_3)COO\}_{16}(H_2O)_4]\cdot 4CH_2C(CH_3)COOH\cdot CH_2Cl_2$.

The activation energy Δ/k_B and the pre-exponential factor τ_0 were estimated to be 66 K and 8.5×10^{-9} s, respectively. These values are close to those observed for other Mn_{12} complexes.[29] The field dependence of the magnetization measured for the cluster (at 1.8 K with a sweep rate of about 50 Oe s^{-1}) reveals a large coercive field around 0.8 T (Fig 4S, ESI). The step feature observed on the curve is probably due to the field reorientation of the crystals under magnetic field. The crystals have not been blocked into a wax but only packed tightly into a plastic bag.

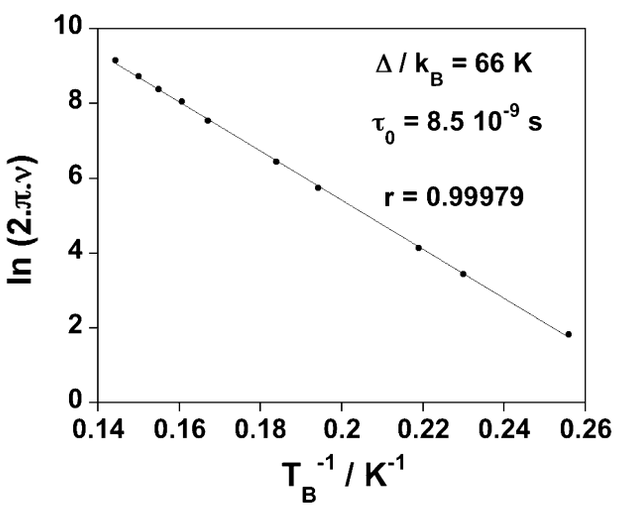

Fig. 5 $\ln(2\pi\nu)$ *vs.* $1/T_B$ plot of $[Mn_{12}O_{12}\{CH_2C(CH_3)COO\}_{16}(H_2O)_4]\cdot 4CH_2C(CH_3)COOH\cdot CH_2Cl_2$. Solid line represents the least-squares fit of the experimental data to the Arrhénius equation.

Synthesis and characterization of the cluster-reinforced copolymers

The copolymerization of $[Mn_{12}O_{12}\{CH_2C(CH_3)COO\}_{16}(H_2O)_4]\cdot 4CH_2C(CH_3)COOH\cdot CH_2Cl_2$ with a 100- to 1000-fold excess of methyl methacrylate initiated by AIBN was performed at 60 °C under vacuum for 48 h using DBPh as a plasticizing agent. The representation of the copolymerization of one of the methacrylate ligands of the cluster with MMA is shown in Scheme 1. The initial concentration of the cluster was varied in order to obtain networks with different amounts of cross-linking agent. In this respect, copolymers with a molar ratio R = MMA/cluster = 100, 200, 300, 500, 800 and 1000 were synthesized. After washing with THF, brown glassy solids with no measurable surface area were obtained. These materials are transparent when the cluster proportion is low, $R > 100$ but become opaque when the cluster proportion is increased ($R = 100$). The experimental conditions were fixed taking into account the solubility and the stability of $[Mn_{12}O_{12}\{CH_2C(CH_3)COO\}_{16}(H_2O)_4]\cdot 4CH_2C(CH_3)COOH\cdot CH_2Cl_2$. The copolymerization may also be performed at lower temperature, *i.e.* 40 °C instead of 60 °C, when the radical initiator Percadox-16S is used instead of AIBN. No difference has been observed in the aspect and physical properties of copolymers obtained using AIBN or Percadox-16S initiators. Finally, a copolymerization performed under heating at 80 °C using dibenzoyl peroxide as initiator led to the homopolymerization of the methyl methacrylate monomer and gave pure poly(methyl methacrylate), accompanied by the partial decomposition of the cluster, which leads to manganese oxide particles.

The presence of the intact cluster core inside the polymer matrixes has been ascertained by infrared spectroscopy (Fig. 5S, ESI). The low frequency bands in the 500–750 cm^{-1} range (456, 512, 543, 588, 632, 712 cm^{-1}), corresponding to Mn–O stretches, along with the bands situated in the 1400–1600 cm^{-1} range, reflecting the carboxylate group vibrations, are present in the Infrared spectra of copolymers, indicating that the intact cluster core is fully conserved within the polymeric matrix. In addition, the strong decrease of the intensity of the ν(C=C) bands indicates that the majority of the peripheral double bonds are involved in the polymerization process and that the cluster is covalently linked to the polymeric matrixes.

Direct evidence that the cluster preserves its structural integrity and its physical properties is given by magnetic measurements. The temperature dependence of the in-phase, χ', and out-of-phase, χ'', ac magnetic measurements for one of the copolymers with $R = 200$ has been obtained in a zero static field with different frequencies ranging from 1 to 1500 Hz (Fig. 6). At 1 Hz, the χ' and χ'' signals exhibit peaks at 5.2 and 4.5 K, respectively. These peaks shift toward higher temperatures when the frequency increases, as also observed in the case of $[Mn_{12}O_{12}\{CH_2C(CH_3)COO\}_{16}(H_2O)_4]\cdot 4CH_2C(CH_3)COOH\cdot CH_2Cl_2$, indicating superparamagnetic-like behaviour. Nevertheless, in contrary to the initial cluster, the copolymer exhibits two relaxation processes, which follow an Arrhenius law with activation energies $\Delta/k_B = 53$ and 21 K and pre-exponential factors $\tau_0 = 5 \times 10^{-8}$ and 2×10^{-8} s for

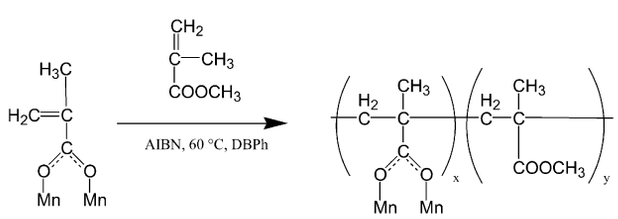

Scheme 1 Schematic representation of the copolymerization of one of the methacrylate ligands of the cluster $[Mn_{12}O_{12}\{CH_2C(CH_3)COO\}_{16}(H_2O)_4]$ with methyl methacrylate.

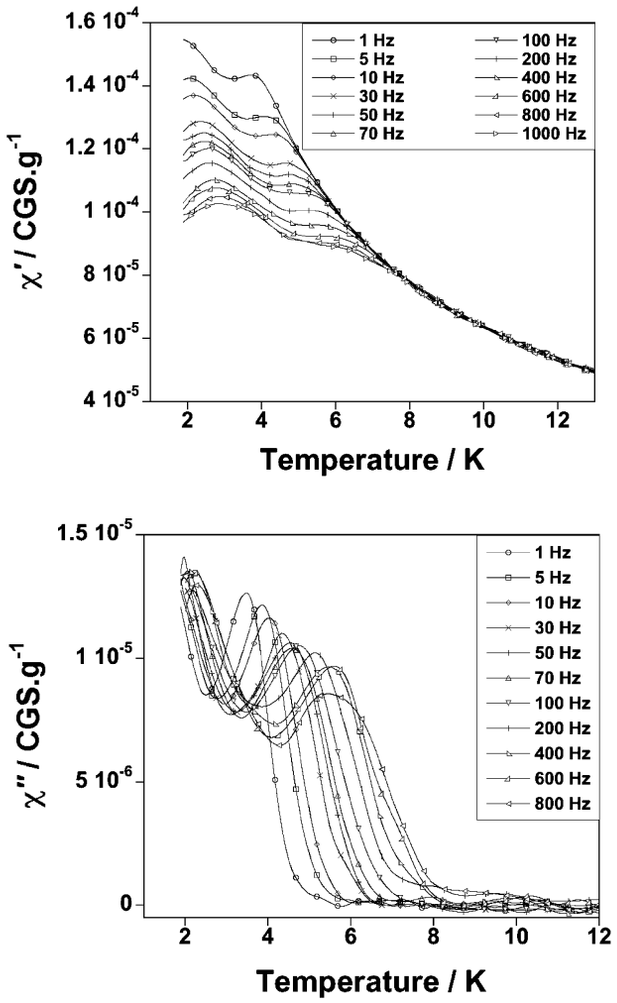

Fig. 6 Temperature and frequency dependence of the (top) real (χ') and (bottom) imaginary (χ'') components of the ac susceptibility for a copolymer with $R = 200$. Measurements for frequencies higher that 1000 and 800 Hz for χ' and χ'', respectively, are not presented due to the important noise observed on the data. Solid lines are guides.

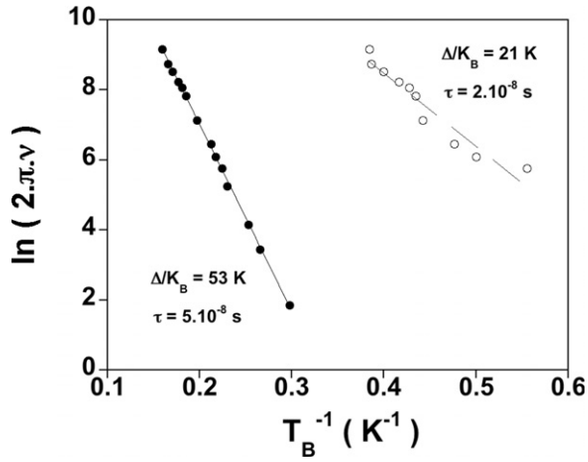

Fig. 7 Ln($2\pi\nu$) *vs.* $1/T_B$ plots for the copolymer with $R = 200$ for both relaxation processes. Solid lines represent the least-squares fits of the experimental data to the Arrhénius equation with $r = 0.999$ for (●) and 0.962 for (○).

the high and low temperature relaxation, respectively (Fig. 7). The parameters of the high temperature relaxation are close to those observed for the initial cluster. The second low temperature relaxation, which is usually observed in solution measurements for clusters of the type $[Mn_{12}O_{12}(RCOO)_{16}(H_2O)_4]$ with $R = CH_3$, C_2H_5, C_6H_6, is attributed to the existence of a Jahn–Teller isomeric form of the cluster.[35] The appearance of the low temperature relaxation may be assigned to a change of the cluster environment related to the covalent bonding of the cluster to the polymer matrix. Finally, the field dependence of the magnetization for the copolymer $R = 200$ presents a hysteresis loop with a coercive field of 0.1 T at 1.8 K with a sweep rate of about 50 Oe s^{-1}, similar to what was observed for the initial cluster. The measured copolymers ($R = 100$, 300, 500) present similar magnetic properties to those described above. However, magnetic signals for copolymers with a low concentration of the cluster ($R = 800$, 1000) are expected to be very low and cannot be detected. As expected, the intensity of the magnetic signal of the copolymers decreases as the amount of cluster in the copolymers decreases without significant modifications of the magnetic properties. Clearly, the magnetic properties of the cluster engaged in the cross-linking knots are expressed through the diamagnetic matrixes.

The prepared copolymers show a remarkable chemical stability. $[Mn_{12}O_{12}\{CH_2C(CH_3)COO\}_{16}(H_2O)_4]\cdot 4CH_2C(CH_3)COOH\cdot CH_2Cl_2$, as all clusters of this family, is sensitive to humidity and instantly decomposes in water. In sharp contrast, the aspect of the copolymers, their infrared spectra and their physical properties did not change when they were stored in a humid atmosphere or even were placed in water for a prolonged period of time. These facts clearly indicate that the magnetic clusters are enwrapped inside the polymeric matrix, which plays a protective role and provides chemical stability.

Higher thermal stability of the copolymers in comparison to the individual cluster is also observed. Pure PMMA degrades in a unique step with an inflexion point at 273 °C and it does not leave any appreciable residue. The thermogravimetric curves for all obtained copolymers performed in the range 0–700 °C with a heating rate of 2 °C min^{-1} are shown in Fig. 8. All of them show three weight loss steps with inflection points at about 200, 380 and 520 °C, determined as the maxima of the first derivative. When the thermogravimetric curves of the copolymers and the individual cluster (Fig. 3) are compared, it is seen that the start of thermal decomposition of the copolymers appears to be shifted by *ca.* 40 °C to higher temperatures. The first weight loss step on the thermogravimetric curves of the copolymers shifts slightly to higher temperatures as the amount of cluster decreases and the temperature of the inflexion point is shifted from 195 to 211 °C as R varies from 100 to 1000. Similarly, a shift to higher temperatures, as the

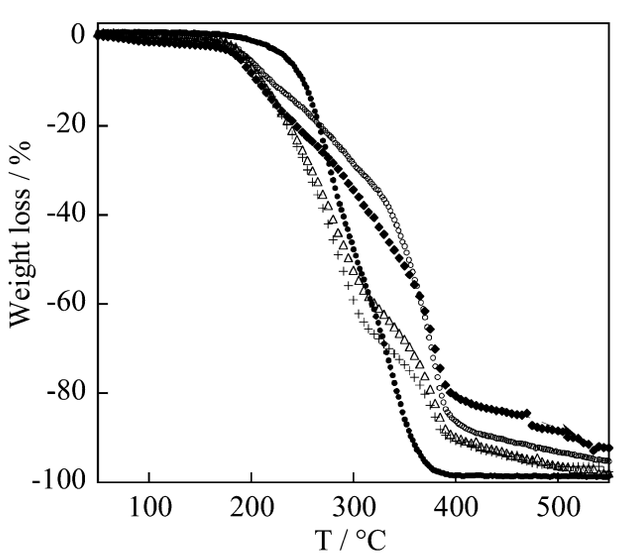

Fig. 8 Thermogravimetric analyses of PMMA (●), the copolymer $R = 100$ (◆), the copolymer $R = 200$ (○), the copolymer $R = 800$ (▽) and the copolymer $R = 1000$ (+).

amount of cluster decreases, is observed for the second and third steps. Heating of the copolymers up to 700 °C leads to Mn_3O_4 as residue. The amount of Mn_3O_4 in these residues corresponds to the expected amount of the cluster present in the copolymers, that is, 7.4, 3.8, 2.8, 1.7, 1.1 and 0.9% for $R = 100$, 200, 300, 500, 800 and 1000, respectively.

The degree of homogeneity of the above copolymeric materials was determined by DSC. Commonly, the characterization of the homogeneity of copolymers by means of DSC relies on the presence or absence of several (or even a continuous distribution of) glass transitions. In other words, it is related to the possibility of rearrangements of each component of the system in order to form either a random copolymer or a segmental copolymer containing a distribution of different polymer segments enriched in one particular component. In the first case, only a single glass transition temperature may be observed. In the second case, several glass transitions corresponding to the distribution of different components may occur.[36] Fig. 9 shows typical DSC curves for the first (top) and second (bottom) heating of the copolymer $R = 200$ performed from 0 to 150 °C. The DSC curves of the obtained copolymers ($R = 100$–1000) present a similar behaviour. The curve of the first heating exhibits an exothermic peak at 105 °C. The enthalpy change associated with this exothermic peak is 16.8 J g^{-1}. It should be noted that similar DSC events were already observed in the study of PMMA copolymers reinforced with titanium clusters and were ascribed to the decomposition of ligated organic molecules.[13] In our case, the first step of the thermal decomposition of cluster-reinforced copolymers determined from the thermogravimetric analysis is around 200 °C. This value is higher than the temperature of the peak observed in DSC. For this reason, this peak may be ascribed to residual cross-linking. It has been confirmed by IR spectroscopy, which shows that after heating samples of the copolymers to 105 °C, no residual ν(C=C) bands were observed, indicating that all double bonds were involved in the polymerization process. The DSC curve of the second heating (Fig. 9, bottom) presents a single T_g at 109 °C showing the formation of the random copolymer. It should be noted that the third heating presents an identical DSC curve, showing that the glass transition is reversible and that no decompositions occurs.

A useful method to estimate the interactions in copolymers between their components is the determination of T_g as a function of the composition. Pure PMMA presents a single glass transition at 83.9 °C. The T_g values of the copolymers as a function of the amount of the cluster decrease as R increases and even for the copolymer $R = 1000$, this value is higher than the one of PMMA (Fig. 6S, ESI). This finding clearly indicates that the chain mobility of PMMA was reduced due to cross-linkage with the cluster.

TEM analyses were performed in order to obtain some information about the homogeneity of the copolymer samples. Indeed, the manganese oxide particles, which may be provided by decomposition of the cluster molecules,[33] and the aggregation of the clusters may be easily detected by the TEM measurements.[21b] The TEM image of the copolymer samples shows homogeneous polymer surfaces and no visible particles or cluster aggregates were observed.

The formation of a cross-linked network for the above copolymers has also been established from their swelling behaviour. The swelling properties of any polymer network depend upon the nature of the polymer, the polymer-solvent compatibility and the degree of cross-linking. Undoped PMMA or PMMA containing mechanically dispersed clusters of $[Mn_{12}O_{12}(O_2CC_2H_5)_{16}(H_2O)_4]$ dissolve completely in CH_2Cl_2 and other common organic solvents such as CH_3CN or toluene. The obtained cluster-reinforced copolymers are insoluble in organic solvents (CH_2Cl_2, CH_3CN, THF, toluene) and only swell to form a persistent gel. Swelling properties are usually characterized by the degree of swelling (I_{sw}, %), which corresponds to the weight of solvent that the dry material is able to absorb. A high degree of swelling is observed in solvents where both PMMA and the cluster are soluble (for example CH_2Cl_2, CH_3CN). Swelling data obtained in the case of CH_2Cl_2 (Fig. 10) show that I_{sw} increases as the R = MMA/cluster ratio increases ($R = 100$–800) and the extent of copolymer swelling depends on the cross-linking density, which itself depends on the amount of functionalized cluster. Indeed, the cross-linking density is increased as the amount of $[Mn_{12}O_{12}\{CH_2C(CH_3)COO\}_{16}(H_2O)_4]$ in the copolymers is increased. In sharp contrast, in solvents such as THF, in which only PMMA is soluble and the cross-linked cluster is insoluble, the degree of swelling is significantly lower; it is five times smaller than in the case of CH_2Cl_2 (Fig. 10). Such an influence of the solvent nature on the swelling of the copolymers requires a substantial contribution of the cluster to the swelling properties.

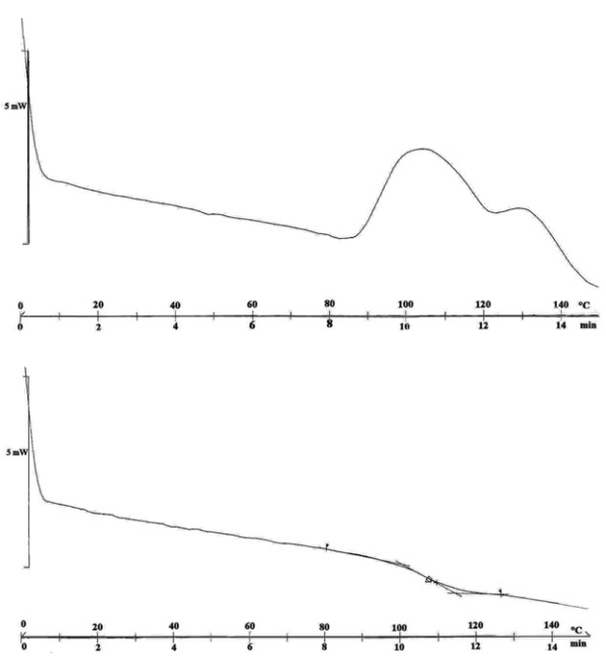

Fig. 9 DSC curves during the first (top) and second (bottom) heating of the copolymer $R = 200$.

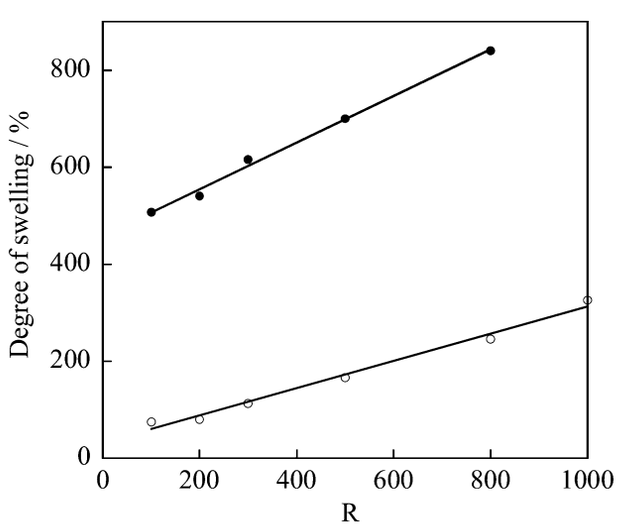

Fig. 10 Degree of swelling as a function of the ratio R in CH_2Cl_2 (●) and THF (○).

Conclusion

In summary, the use of functionalized molecular clusters with tailored physical properties as the cross-linker in copolymerization with organic polymers appears to be a promising route to covalently bonded polymer-based nanocomposites. In this work, we have synthesized a new methacrylate-functionalized manganese carboxylate cluster $[Mn_{12}O_{12}\{CH_2C(CH_3)COO\}_{16}(H_2O)_4]$ exhibiting SMM properties *via* a ligand exchange reaction. This cluster has been fully characterized by X-ray diffraction, mass spectrometric and magnetic analyses. We have used this precursor as cross-linker in free radical polymerization with methyl methacrylate in order to form hybrid copolymer networks and we have obtained a series of copolymers with 0.1–1 mol % of cluster ($R = 100$–1000).

A first observation is that in these nanocomposites, the polymeric matrix enwraps and protects the manganese carboxylate cluster, which improves its chemical and thermal stability. The magnetic properties of the individual cluster have been preserved and transferred to the copolymer materials. It should be noted that the structural integrity and the physical properties of the cluster are preserved after copolymerization.

The second point is that the pre-functionalized cluster acts as an efficient cross-linker agent for the polymer chains, allowing the formation of highly cross-linked networks. The formation of covalent bonds between the cluster and the PMMA allows random copolymers to be obtained in which the ratio MMA/cluster is controlled. These hybrid copolymers present swelling behaviour and form a persistent gel.

Finally, the preparation of thin polymeric films containing the magnetic cluster is under progress. Moreover, the number of polymerizable functionalities of the manganese carboxylate cluster can be changed and may allow us to modify the morphology and physical properties of the cluster-reinforced copolymers.[34]

Acknowledgements

This work was supported by the CNRS, the University of Montpellier II, the University of Bordeaux I and the Conseil Regional d'Aquitaine. The authors thank Dr. Y. Guari for TEM measurements and helpful discussions.

References

1 Special Issue on Nanostructured Materials: *Chem. Mater.*, 1996, 8(8), 1569–2194 and references therein.
2 (*a*) L. L. Beecroft and C. K. Ober, *Chem. Mater.*, 1997, **9**, 1302; (*b*) I. A. Akimov, I. Y. Denisyuk and A. M. Meshkov, *Opt. Spectrosc.*, 1992, **72**, 558; (*c*) S.-H. Yu, Y. Yoshimura, J. M. Calderon Moreno, T. Fujiwara, T. Fujino and R. Teranishi, *Langmuir*, 2001, **17**, 1700; (*d*) J. Y. Wang, W. Chen, A.-H. Liu, G. Lu, G. Zhang, J. H. Zhang and L. Yang, *J. Am. Chem. Soc.*, 2002, **124**, 13 358; (*e*) J. G. Winiarz, L. Zhang, J. Park and P. N. Prasad, *J. Phys. Chem. B*, 2002, **106**, 967; (*f*) M. Wang, H.-G. Bram and E. Meyer, *Chem. Mater.*, 2002, **14**, 4812; (*g*) Y. Lin, B. Zhou, K. A. Shiral Fernando, P. Liu, L. F. Allard and Y. P. Sun, *Macromolecules*, 2003, **36**, 7199; (*h*) D. K. Lee, Y. S. Kang, C. S. Lee and P. Stroeve, *J. Phys. Chem. B*, 2002, **106**, 7267.
3 (*a*) J. K. Vassilion, R. P. Ziebarth and F. J. Disalvo, *Chem. Mater.*, 1990, **2**, 738; (*b*) P. C. Morais, R. B. Azevedo, D. Rabelo and C. D. Lima, *Chem. Mater.*, 2003, **15**, 2485; (*c*) B. Lindlar, M. Boldt, S. Eiden-Assmann and G. Maret, *Adv. Mater.*, 2002, **14**, 1656; (*d*) M. Breulmann, H. Gölfen, H.-P. Hentze, M. Antonetti, D. Walsh and S. Mann, *Adv. Mater.*, 1998, **10**, 237; (*e*) C. Castro, J. Ramos, A. Millan, J. Gonzales-Calbet and F. Palacio, *Chem. Mater.*, 2000, **12**, 3681; (*f*) M. Zrinyi, *Colloid. Polym. Sci.*, 2000, **278**, 98; (*g*) R. Gangopadhyay and A. De, *Chem. Mater.*, 2000, **12**, 608.
4 (*a*) S. A. Davis, M. Breulmann, K. H. Rhods, B. Zhang and S. Mann, *Chem. Mater.*, 2001, **13**, 3218; (*b*) D. Leun and A. K. Sengupta, *Environ. Sci. Technol.*, 2000, **34**, 3276.
5 G. Cao, M. E. Garcia, M. Aleala, L. F. Burgess and T. E. Mallouk, *J. Am. Chem. Soc.*, 1992, **114**, 7574.
6 (*a*) M. Z. Rong, M. Q. Zhang, H. O. Liang and H. M. Zeng, *Chem. Phys.*, 2003, **286**, 267; (*b*) S. Yang, Y. Horibe, C.-H. Chen, P. Mirau, T. Tatry, P. Evans, J. Grazul and E. M. Dufresne, *Chem. Mater.*, 2002, **14**, 5173; (*c*) R. B. Thompson, V. V. Ginzburg, M. W. Matsen and A. C. Balazs, *Macromolecules*, 2002, **35**, 1060; (*d*) F. Grohn, B. J. Bauer, Y. A. Akpalu, C. L. Jackson and E. J. Amis, *Macromolecules*, 2002, **35**, 6042.
7 H.-L. Tasi, J. L. Schindler, C. R. Kannewurf and M. G. Kanatzidis, *Chem. Mater.*, 1997, **9**, 875.
8 C Sanchez, G. J. de, A. A. Soler-Illia, F. Ribot, T. Lalot, C. R. Mayer and V. Cabuil, *Chem. Mater.*, 2001, **13**, 3061 and references therein.
9 U. Schubert, *Chem. Mater.*, 2001, **13**, 3487 and references therein.
10 (*a*) A. R. Moore, H. Kwen, A. M. Beatty and E. A. Maatta, *Chem. Commun.*, 2000, 1793; (*b*) J. Pynn and K. Matyjaszewski, *Macromolecules*, 2000, **33**, 217.
11 F. Ribot, F. Banse, C. Sanchez, M. Lahcini and B. Jousseaume, *J. Sol-Gel Sci. Technol.*, 1997, **8**, 529.
12 (*a*) G. Trimmel, P. Fratzl and U. Schubert, *Chem. Mater.*, 2000, **12**, 602; (*b*) U. Schubert, T. Völkel and N. Moszner, *Chem. Mater.*, 2001, **13**, 3811.
13 (*a*) Y. Gao, N. R. Choudhury, J. Matisons, U. Schubert and B. Moraru, *Chem. Mater.*, 2002, **14**, 4522; (*b*) U. Schubert, N. Hüsing and A. Lorenz, *Chem. Mater.*, 1995, **7**, 2010.
14 L. Xu, M. Lu, B. Xu, Y. Wei, Z. Peng and D. R. Powell, *Angew. Chem., Int. Ed.*, 2002, **41**, 4129.
15 (*a*) C. R. Mayer, R. Thouvenot and T. Lalot, *Macromolecules*, 2000, **33**, 4433; (*b*) C. R. Mayer and R. Thouvenot, *Chem. Mater.*, 2000, **12**, 257; (*c*) P. Judeinstein and C. Sanchez, *J. Mater. Chem.*, 1996, **6**, 511.
16 D. Gatteschi and R. Sessoli, *Angew. Chem., Int. Ed.*, 2003, **42**, 268 and references therein.
17 R. Sessoli, D. Gatteschi, A. Caneschi and M. A. Novak, *Nature (London)*, 1993, **365**, 141.
18 (*a*) L. Krusin-Elbaum, T. Shibauchi, B. Argyle, L. Gignac and D. Weller, *Nature (London)*, 2001, **410**, 444; (*b*) E. M. Chudnovsky and J. Tejeda, *Macroscopic Quantum Tunneling of the Magnetic Moment*, Cambridge University Press, Cambridge, 1998.
19 M. Clemente-Leon, H. Soyer, E. Coronado, C. Mingotaud, C. J. Gomez-Garcia and P. Delhaès, *Angew. Chem., Int. Ed.*, 1998, **37**, 2842.
20 D. Ruiz-Molina, M. Mas Torrent, J. Tejada, M. T. Martinez, C. Rovira and J. Veciana, *Adv. Mater.*, 2003, **15**, 42.
21 (*a*) T. Coradin, J. Larionova, A. A. Smith, G. Rogez, R. Clérac, C. Guérin, G. Blondin, R. E. P. Winpenny, C. Sanchez and T. Mallah, *Adv. Mater.*, 2002, **14**, 896; (*b*) S. Willemin, G. Arrachart, L. Lecren, J. Larionova, T. Coradin, R. Clérac, T. Mallah, C. Guérin and C. Sanchez, *New J. Chem.*, 2003, **27**, 1533
22 T. Lis, *Acta Crystallogr., Sect. B*, 1980, **36**, 2042.
23 A. Altomare, M. C. Burla, M. Camalli, G. Cascarano, C. Giacovazzo, A. Guagliardi and G. Polidori, *J. Appl. Crystallogr.*, 1994, **27**, 435.
24 G. M. Sheldrick, *SHELXS-97, Program for solution of crystal structures*, University of Göttingen, Germany, 1997; G. M. Sheldrick, *SHELXL-97, Program for refinement of crystal structures*, University of Göttingen, Germany, 1997.
25 *International Tables for X-Ray Crystallography*, Kynoch Press, Birmingham, England, 1974, vol. IV.
26 M. Nardelli, *J. Appl. Crystallogr.*, 1999, **32**, 563.
27 E. A. Boudreaux, L. N. Mulay, *Theory and Applications of Molecular Paramagnetism*, John Wiley & Sons, New York, 1976.
28 M. Vamvakaki and C. S. Patrickios, *Chem. Mater.*, 2002, **14**, 1630.
29 (*a*) R. Sessoli, H.-L. Tsai, A. R. Schake, S. Wang, J. B. Vincent, K. Folting, D. Gatteschi, G. Christou and D. N. Hendrikson, *J. Am. Chem. Soc*, 1993, **115**, 1804; (*b*) H. J. Eppley, H. L. Tsai, N. De Vries, K. Folting, G. Christou and D. Hendrickson, *J. Am. Chem. Soc.*, 1995, **117**, 301; (*c*) P. Artus, C. Boskovic, J. Yoo, W. E. Streib, L.-C. Brunel, D. Hendrickson and G. Christou, *Inorg. Chem.*, 2001, **40**, 4199.
30 K. Nakamoto, *Infrared and Raman Spectra of Inorganic and Coordination Compounds*, Wiley Interscience, New York, 2nd edn., 1970.
31 (*a*) R. Taylor and O. Kennard, *J. Am. Chem. Soc.*, 1982, **104**, 5063; (*b*) G. R. Desiraju, *Acc. Chem. Res.*, 1996, **29**, 441.

32 D. Ruiz-Molina, P. Gerbier, E. Rumberger, D. B. Amabilino, I. A. Guzei, K. Folting, J. C. Huffmann, A. Rheingold, G. Christou, J. Veciana and D. N. Hendrickson, *J. Mater. Chem.*, 2002, **12**, 1152.
33 B. Boury, J. Larionova, R. Clérac, J. Le Bideau, L. Lecren and S. Willemin, *J. Mater. Chem.*, 2003, **13**, 795.
34 S. Willemin, B. Henner, C. Guérin and J. Larionova, unpublished results.
35 (*a*) Z. Sun, D. Ruiz, N. R. Dilley, M. Soler, J. Ribas, K. Folting, M. B. Maple, G. Christou and D. N Hendrickson, *Chem. Commun.*, 1999, 1973; (*b*) Z. Sun, H. J. Eppley, E. M. Rumberger, I. A. Guzei, K. Folting, P. K. Gantzel, A. L. Rheingold, G. Christou and D. N. Hendrickson, *Inorg. Chem.*, 2001, **40**, 2127.
36 J. L. Gomez Ribelles, M. Monleon Pradas, J. M. Meseguer Duenas and C. Torregrosa Cabanilles, *J. Non-Cryst. Solids*, 2002, **307**, 731.